Registration and motion compensation of a needle placement robot for CT-guided spinal procedures

Sheng Xu[*a], Kevin Cleary[b], Dan Stoianovici[c], and Gabor Fichtinger[a]
[a]Engineering Research Center, Johns Hopkins University, Baltimore, MD, USA 21218;
[b]Imaging Science and Information Systems (ISIS) Center, Department of Radiology, Georgetown University Medical Center, Washington, DC, USA 20007;
[c]James Buchanan Brady Urological Institute, Johns Hopkins Medical Institutions, Baltimore, MD, USA 21224

ABSTRACT

Computed tomography (CT) guided needle placement is an established practice in the medical field. The efficacy of these procedures is related to the accuracy of needle placement. Current free-hand techniques have limitations in accuracy, which is often affected by the patient motion. In response to these problems and as a testbed for future developments, we propose a robotically assisted needle placement system consisting of a mobile CT scanner, a needle insertion robot, and an optical localizer. This paper presents the overall system concept and concentrates on the system registration and compensation of the patient motion. Accuracy results using an abdominal phantom are also presented.

Keywords: Image guidance, medical imaging, medical robotics, needle placement, registration, tracking

1. INTRODUCTION

1.1 Clinical significance

Spinal disorders are the fastest growing musculoskeletal subspecialty. It is estimated that over 70% of the population experiences significant low-back pain during their lives. Recent advances in medical imaging have propelled minimally invasive image-guided biopsy and local therapies into public attention[1]. Computed tomography (CT) guided nerve blocks and facet joint injections have proven to be safe and effective methods to treat spinal pain[2].

Currently, percutaneous (through the skin) placement of needles into the spine is performed freehand. Based on CT or fluoroscopy, the physician identifies the skin entry point and the target, thus defining the desired needle trajectory. The physician then aligns the needle by hand and advances it towards the target gradually while checking the position of the needle by re-imaging as necessary. The main problem is that the physician has limitations in accuracy when initially lining up the needle and subsequently staying on course. In addition, motion of a lumbar vertebral body due to breathing alone is up to 1.3 mm (peak to peak), and surgeon-induced motion up to ten times greater[3]. When the physician releases the needle, the needle can drift or tilt away from the desired path. In response to these problems, we propose integrating intra-operative CT imaging with a medical robot for precise placement of the needle.

The workflow of the current manual procedure is practically identical to the steps followed by our robotic system. This parallelism offers a unique opportunity for gradual transition from a manual procedure to a fully robotic intervention. While experienced physicians can complete these procedures without difficulty, there is a need for precise and consistent aiming and delivery of the needle. The longevity of pain relief is thought to be associated with the spatial accuracy of needle placement. The system can also serve as a testbed for the precise robotically guided needle placement systems of the future.

1.2 Prior technical developments

The history of medical robotics dates back to 1985, when Kwoh applied a PUMA robot to orient a needle for biopsy of

[*] sheng@cs.jhu.edu; phone 1 410 516-4318; fax 1 410 516-5553

Medical Imaging 2005: Visualization, Image-Guided Procedures, and Display, edited by Robert L. Galloway, Jr., Kevin R. Cleary, Proc. of SPIE Vol. 5744 (SPIE, Bellingham, WA, 2005) · 1605-7422/05/$15 · doi: 10.1117/12.594731

the brain[4]. Other early work with needle placement robots was also focused on intra-cranial neurosurgery[5-7]. Since then, however, many other clinical applications for needle placement robots have now been proposed, such as the AESOP robot from Computer Motion, a voice activated endoscopic camera holder used in abdominal interventional procedures[8]. Taylor pioneered the application of the remote center of motion (RCM) concept for needle placement, which provides rotational motion around a fixed fulcrum point in space. Taylor developed the first such robot for manipulation of laparoscopic instruments[9]. Loser presented a lightweight 5-bar RCM linkage for needle insertion[10] that was guided by visual servoing in a CT fluoroscopy scanner. Stoianovici developed a two degrees-of-freedom (DOF) RCM robot with a radiolucent needle driver for percutaneous renal access under fluoroscopic guidance[11, 12]. Taylor and Stoianovici also adapted the RCM module for microsurgical augmentation[13].

In addition to these hardware developments, many researchers have attempted to integrate the robotic system with the guiding imaging modality. Yanof[14] integrated an industrial robot arm for needle placement with a CT scanner and completed swine animal studies. Masamune[15] integrated Stoianovici's RCM-PAKY robot and Susil's stereotactic registration method[16] for needle insertion inside a CT scanner. Fichtinger adapted this system for transperineal access to the prostate under intra-operative CT guidance[17].

1.3 Significance of this paper

The system presented here employs the 6-DOF Acubot robot described in[18]. The robot includes a 3-DOF translational stage, a 2-DOF orientation module, and a 1-DOF needle driver. A real-time optical localizer (Polaris, Northern Digital, Waterloo, Canada) is incorporated in the system, allowing continuous measurement of the relative locations of the robot and patient. This allows the system to automatically compensate for patient motion.

Real-time tracking of surgical instruments and imaging devices has been applied routinely in image-guided surgery (IGS) systems for navigation purposes. In the spine, pioneering work has been done by Nolte[19] and Lavallee[20]. The motion of the lumbar spine in the prone position during pedicle screw placement in open surgery has been studied by Glossop[3]. Several aspects of our tracking method are directly inspired by these systems, including the use of optical tracking and the assumption that the vertebral body behaves as a rigid body.

The novel aspects of this paper are the following: (1) automated registration between the robot, patient and CT images based on an optical tracking system and an embedded fiducial device, (2) nearly real-time tracking of the patient, (3) the implementation of a control loop to compensate for displacement of the target due to respiratory motion or patient movement during the intervention.

2. SYSTEM COMPONENTS

2.1 Clinical workflow

The main system components are shown in Figure 1. The intra-operative scenario for robotically assisted biopsy or therapy is as follows:

1. The patient is positioned on the table.
2. The robot is mounted over the patient and calibrated.
3. The patient is scanned and the images are sent to the control computer for the system.
4. The physician selects the entry and target locations.
5. The robot moves the RCM center to the entry point.
6. The robot orients the needle to the target point.
7. The robot starts tracking the target location and compensates for patient motion as required.
8. The robot inserts the needle to the predefined depth.
9. Another CT scan is done for verification.
10. The physician injects the therapeutic agent or takes the biopsy sample.
11. The robot retracts the needle.

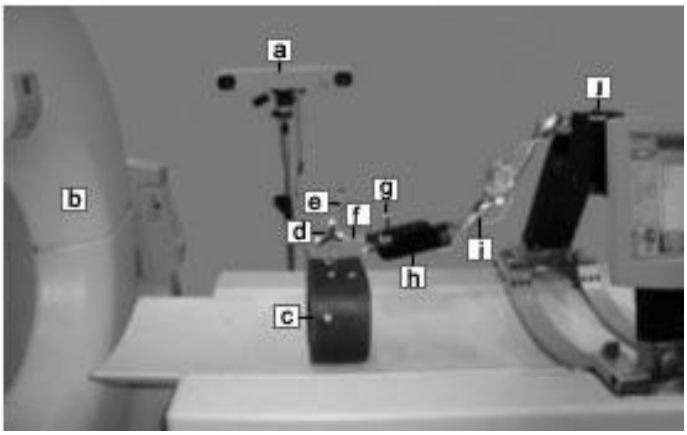

Figure 1: System components: (a) Polaris (b) CT gantry (c) Abdominal phantom (d) Fiducial carrier (e) Needle (f) Needle driver (g) Robot tracker (h) RCM (i) Passive arm (j) Cartesian bridge

Figure 2: User interface (Slicer) with path planning

The "point-and-click needle placement" paradigm is implemented in the system, where the physician selects the entry and target points on a computer screen, and an autonomous robot executes the needle placement under the supervision of the physician. In order to increase safety, the needle is retracted from the RCM center during the tracking to avoid any possible collision with the patient.

2.2 Planning and monitoring software

The system was tested using a mobile CT scanner (Tomoscan, Philips Medical Systems, Eindhoven, Netherlands) and an abdominal interventional phantom (CIRS Inc., Norfolk, Virginia). The images are transferred from the CT scanner to the robot control computer over an Ethernet connection using the DICOM protocol. The planning and control software is based on 3D Slicer[21], a free open-source software package for visualization, registration, and quantification of medical data.

As shown in Figure 2, 3D Slicer was modified to provide the following capabilities: (1) a path planning interface for the user to select the skin entry point and target point, which can be on different axial slices; (2) control and monitoring of the robot; and (3) control and display for the Polaris localizer. The software was developed using Tcl/Tk and the Visualization Toolkit (VTK).

2.3 Needle placement robot and control software

Manual needle punctures usually include three decoupled motions. First, the tip of the needle is moved from its current location to the skin entry point. This is a three-dimensional Cartesian motion. Second, the needle is oriented by pivoting around the skin entry point. This motion involves two independent rotations. Finally, one-directional translation is necessary to insert the needle into the body through the skin. Therefore, needle placement requires 3+2+1=6 degrees of freedom.

This kinematic arrangement is realized in the Acubot robot used here[18]. Acubot contains a 3-DOF Cartesian motion stage mounted over the CT table. The maximum speed of the Cartesian stage is 20mm/s for each of the three translation axes. The Cartesian stage is connected to a 7-DOF adjustable unencoded passive arm, used for gross positioning of the needle drive stage. The rotation stage is a 2-DOF RCM with maximum speeds of 37°/sec and 74°/sec respectively. The needle drive stage is a 1-DOF friction transmission with a radiolucent end-effector for insertion of the needle.

The control electronics for the robot are housed entirely within a single industrial PC chassis. Safety features include

current monitoring and a watchdog timer. The software used to control the robot is the modular robot control library (MRC), which has been developed at the Johns Hopkins University.

3. COORDINATE TRANSFORMATIONS AND ROBOT MOVEMENT

The key to accurate needle placement is the precise real-time computation of the coordinate transformations between the robot, patient, and images. Figure 3 shows the five coordinate systems involved in the computation. The Polaris is used to track patient motion in real-time and to register the robot to the coordinate system of the CT scanner and patient. Since the Polaris coordinate system is the only stationary coordinate system, every other coordinate system is registered to the Polaris coordinate system. The needle placement task requires that the robot first moves the RCM center to the skin entry point and then orients the needle before driving the needle to the target.

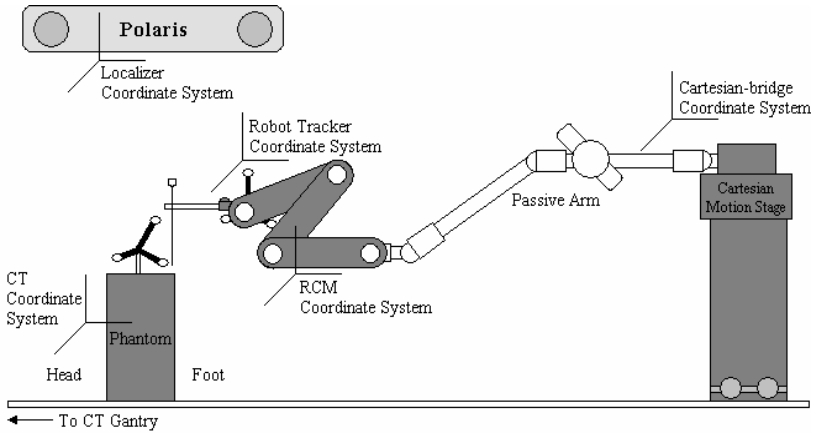

Figure 3: Coordinate systems

Figure 4: Interventional phantom with fiducial carrier

3.1 Movement to skin entry point

To move the RCM center of the robot to the skin entry point, the following steps are required.

3.1.1 Registration of CT to Polaris

A rigid plastic fiducial carrier (Figure 4, PassTrax, Traxtal Technologies, Toronto, Canada) is attached to the vertebral body of an abdominal phantom. This carrier contains three retro-reflective spheres (seen by the Polaris) and nine 0.8 mm radiodense microspheres (Tilly Medical, Lund, Sweden) placed in a known and precise arrangement. Using this fiducial carrier, the computer can determine the position of the nine microspheres in both the Polaris and CT coordinate systems. Arun's singular value decomposition (SVD) technique[22] is used to determine the transformation matrix between the Polaris and CT coordinate systems. The entry and target points can therefore be transformed from the CT to the Polaris coordinate system.

3.1.2 Registration of RCM center to Polaris

A single passive marker is placed on the needle during a pre-procedure calibration phase as shown in Figure 5. A fulcrum motion is executed using the RCM stage, while the Polaris is tracking the marker on the needle. Then the needle is moved forward some distance and the same fulcrum motion is repeated. The tip of the cone defined by the two trajectories of the marker yields the RCM point in Polaris space.

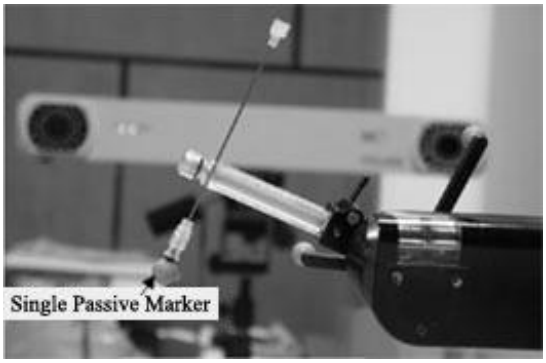

Figure 5: Needle with a passive marker on its tip

3.1.3 Registration of Cartesian bridge to Polaris

The rotational transformation between the Cartesian motion stage and the Polaris is computed using the robot tracker. The robot tracker is an optical tracker rigidly attached to the last link of the robot. The combination of the robot tracker and Cartesian motion stage can be considered a rigid body for pure translations. The Cartesian motion stage is moved to the eight vertices of its maximum workspace (a rectangle of 200 by 40 by 40 mm), and positional data is simultaneously recorded in the coordinate systems of the Cartesian stage and Polaris tracker. As in step 1, the rotation matrix between the two coordinate systems is then determined using the SVD.

3.1.4 Needle movement

The desired needle movement is from the initial position of the needle tip to the entry point. The corresponding motion of the Cartesian stage can be determined using the above transformations.

3.2 Orientation of needle

The following steps are required to orient the needle along the desired path.

3.2.1 Registration of needel orientation to Polaris

Similar to Step 2 of Section A, a single passive marker is placed on the needle during the pre-procedure phase and the RCM stage is set to its home orientation. The needle is driven up and down without changing the orientation of the robot, while the Polaris records the marker position. The orientation of the needle is then calculated using 3D line fitting.

Since the robot tracker is secured to the needle driver, both the needle orientation and the initial position of the needle tip are constant in the robot tracker coordinate system. Therefore, they can be saved as system constants after the registration is performed for the first time. Their corresponding orientation and position in the Polaris coordinate system can be calculated using the transformation between robot tracker and Polaris.

3.2.2 Registration of RCM stage to Polaris

The rotational transformation between the RCM stage and Polaris is determined using the robot tracker. Using the orientation of the robot tracker before and after a rotation about a single RCM joint, the rotation axis of each joint can be calculated directly in the Polaris coordinate system[23]. The rotation matrix between RCM and Polaris is therefore obtained after both RCM axes are determined.

3.2.3 Needle orientation

Using the results above, both the initial needle orientation and the desired path vector can be transformed to the RCM coordinate system. The inverse kinematics of the RCM is then applied to orient the needle to the path.

3.3 Track and compensate patient motion

To track and compensate the motion of the patient, a control loop is executed in the software. The needle is retracted from the RCM center to avoid any potential collision with the patient during the tracking. The following steps are executed inside the loop:

1. Read the location of the phantom (patient) tracker using the Polaris.
2. Register CT images to the Polaris with the new posture of the patient obtained in step 1.
3. Update the path vector (the entry point and the target point) in the Polaris coordinate system with the new transformation obtained in step 2.
4. Move the needle tip to the updated skin entry point and align the needle with the updated path vector.

In the second step, since the patient's motion doesn't change the relative position of the microspheres with respect to the target, the registration described in section III-A/1 is not repeated. This saves a large amount of CPU time and makes real-time tracking and compensation possible, although our current implementation is not optimized for this purpose.

4. EXPERIMENTAL RESULTS

An abdominal interventional phantom (CIRS Inc., Norfolk, VA) with both surface and internal fiducials was CT scanned with 1.0 mm slice thickness and 0.742 mm pixel size. The passive arm was positioned in an arbitrary position such that the phantom was within the workspace of the robot and the field of view of the Polaris. The maximal speed of the robot was set at 10 mm/s for each of the Cartesian joints and 5°/s for each of the RCM joints, with maximal acceleration 3 mm/s^2 and $5°/s^2$ respectively. The update rate of the system was a relatively slow 2Hz, which was due to the overhead of the software components involved.

4.1 Translation accuracy

The accuracy of guiding the needle tip to the entry point was determined using a needle with a single passive marker on its tip. According to the manufacturer, the root-mean-square (RMS) error of the Polaris when tracking a single passive marker is 0.35 mm. After registration, a sample entry point was identified in the CT image. This entry point was selected in air above the phantom to avoid a potential collision between the passive marker and the phantom. The Cartesian stage was commanded to move the needle tip from its current position to the entry point. The position of the passive marker was recorded and then transformed back to the CT coordinate system. In the translation tests, the average translation of the robot was 31.2mm. The results are shown in Table 1.

In the above procedure and the following one in IV-B, both the forward and inverse transformations between CT and Polaris were involved in the measurements. Therefore, the results did not reflect the accuracy of CT-Polaris registration. This accuracy was determined by two factors: (a) the intrinsic 0.35 mm RMS error of the Polaris and (b) the error of image-based detection of microspheres in the fiducial carrier, evaluated by the Fiducial Registration Error (FRE) formula[24], which yielded 0.26 mm for the nine microspheres.

Table 1: Translation and orientation accuracy

Number of translation tests	20
Mean position error	0.5 mm
STD of position error	0.2 mm
Number of orientation tests	20
Mean orientation error	0.7°
STD of orientation error	0.4°

Table 2: Overall system accuracy

Number of static tests	5
Mean static error	1.0 mm
STD of static error	0.3 mm
Number of dynamic tests	6
Mean dynamic error	1.7 mm
STD of dynamic error	0.4 mm

4.2 Orientation accuracy

As in task A, a single passive marker was placed on the needle tip to evaluate the alignment of the needle with the desired path vector. After the needle was aligned with the path, it was driven up and down and the Polaris recorded the position of the passive marker continuously. Using 3D line fitting, the needle vector in the Polaris coordinate system was obtained. The needle vector was transformed back to the CT coordinate system and compared with the desired path vector. The results are shown in Table 1.

4.3 Overall system accuracy

The system accuracy was estimated statically and dynamically using a digital camera (Canon PowerShot G2). Several 1.0 mm diameter lead balls were attached on the phantom surface as target points for the robot. The entry point was selected in the air above the phantom and the target point was one of the lead balls. In the static test, after the registration step, the robot moved the needle tip to an entry point and aligned the needle with the desired path. The needle tip was then driven from the RCM center to the target point until the needle tip was closest to the fiducal (or touched it). The error between the actual driven distance and the length of the desired path was recorded. Two orthogonal pictures were taken with the digital camera and a ruler in the field of view as shown in Figure 6. The angle between the needle and the phantom surface was estimated to calculate the error in the plane perpendicular to the needle. The dynamic test was almost the same as the static test except that every time the phantom was moved to an arbitrary new position and re-registered. In both static and dynamic tests, the insertion angles were uniformly selected in the robot's workspace. The needle tip translation ranged from 17.0 mm to 47.4 mm. The insertion depth ranged from 34.8 mm to 60.1 mm. Table 2 shows the estimation of the overall system accuracy.

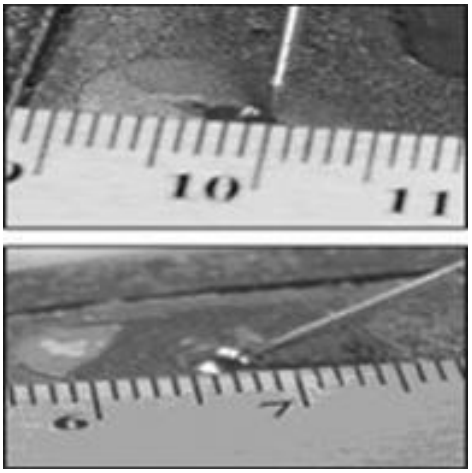

Figure 6: Orthogonal views of needle touching a fiducial (ruler unit 1mm)

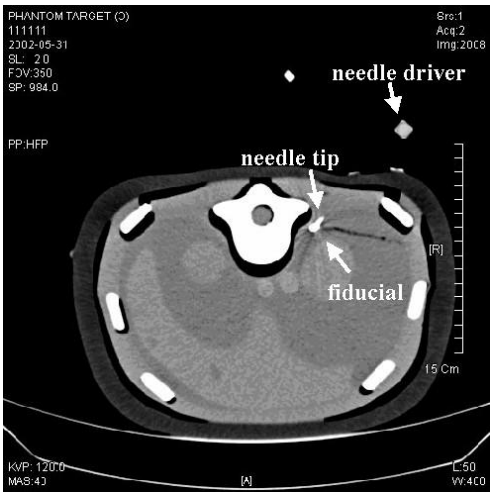

Figure 7: Accuracy test and internal fiducial

To test the system on an internal target point, a fiducial was also implanted as the target point at a clinically representative location inside the phantom. Since the phantom was made from foam and rubber and the perispinal targets were relatively superficial, the effects of tissue-needle interaction forces were believed to be small. Figure 7 shows a confirmatory CT image with the needle directly touching the implanted fiducial. The planned path to the metal ball was on an oblique plane, passing through twelve axial 1 mm CT slices.

5. DISSCUSSION

The system presented here is intended to demonstrate the concept of registration of a needle placement robot with the patient's anatomy, and the potential for compensation of intra-operative motion. The phantom studies showed that the

system has reasonable accuracy. Although the system is relatively slow in compensating for motion, the concept of motion compensation has been demonstrated. Several weaknesses of the system are as follows.
The system did not achieve a sufficiently large working volume, mainly due to interference between the trackers and the patient body. The dimensions of the fiducial carriers need to be reduced and relocated both on the robot and the patient to alleviate this interference problem. The fiducial carrier and associated locking pin attached to the spinous process is rather large and more invasive than desired in the clinical setting.

The current needle driver uses a friction transmission that has a limited exertion force. If the resistance of the tissue is greater than the maximum transmission force, the needle will slip and stop short of the target. Using a spinning needle injector may help alleviate this problem[12].

The current end-effector cannot automatically release the needle if excessive force or movement is detected. This is a potential safety problem if the control system cannot rapidly detect and compensate for involuntary movement of the patient.

In conclusion, this paper showed the feasibility of the overall concept and demonstrated reasonable accuracy in phantom trials. Several weaknesses were identified that need to be resolved before an automated needle placement robot system can be proposed for human trials.

ACKNOWLEDGEMENT

The work was supported by the following organizations: (1) U.S. Army grant DAMD17-99-1-9022, (2) National Science Foundation under the Engineering Research Center grant #EEC 9731478, (3) Whiting School of Engineering and Brady Urological Institute of the Johns Hopkins University. The authors gratefully acknowledge the longstanding support and advice of Louis R. Kavoussi, M.D. (Brady Urological Institute) and Russell H. Taylor, Ph.D. (Engineering Research Center), both at the Johns Hopkins University. We also thank David Lindisch, RT, for his assistance with the experiments at Georgetown University.

REFERENCES

1. R. K. Jain, “The next frontier of molecular medicine: Delivery of therapeutics”, Nature Medicine, **4**, pp. 655-657, 1997.
2. A. Gangi, J. L. Dietemann, R. Mortazavi, D. Pfleger, C. Kauff and C. Roy, “CT-guided interventional procedures for pain management in the lumbosacral spine”, Radiographics, **18**(3), pp. 621-633, 1998.
3. N. Glossop and R. Hu, "Assessment of vertebral body motion during spine surgery”, Spine, **22**(8), pp. 903-909, 1997.
4. Y. S. Kwoh, J. Hou, E.A. Jonckeere and S.Hayati, “A robot with improved absolute positioning accuracy for CT guided stereotactic brain surgery”, IEEE Trans. on Biomed. Eng., **35**(2), pp. 153-160, 1988.
5. J.M. Darke, M. Joy, A. Goldenberg, et. al. “Computer and robotic assisted resection of brain tumors”, Proc. 5th Int. Conf. on *Advanced Robotics*, pp. 888-892, 1991.
6. D. Glauser, H. Fankhauser, M. Epitaux, J. L. Hefti, and A. Jaccottet, “Neurosurgical robot Minerva: first results and current developments”, J. Image Guid. Surg., **1**(5), pp. 266-272, 1995.
7. K. Masamune, L. H. Ji, M. Suzuki, T. Dohi, H. Iseki, K. Takakura, “A Newly Developed Stereotactic Robot with Detachable Drive for Neurosurgery”, *Lecture Notes in Computer Science*, Proc. of MICCAI’98, pp. 215-222, 1998.
8. Surgical robotics, “Evaluation of the Computer Motion AESOP 3000 robotic endoscope holder”, Health Devices, **31**(7), pp. 256-268. July 2002.
9. R. H. Taylor, J. Funda, B. Eldridge, K. Gruben, D. LaRose, S. Gomory, M. Talamini, L. Kavoussi, J. Anderson, "A Telerobotic Assistant for Laparoscopic Surgery", IEEE EMBS Magazine Special Issue on Robotics in Surgery, pp. 279-291, 1995.

10. M. Loser and N. Navab, “A new robotic system for visually controlled percutaneous interventions under CT Fluoroscopy”, MICCAI 2000, *Lecture Notes in Computer Science*, Springer Verlag, vol. 1935, pp 887-896, 2000.
11. D. Stoianovici, J. A. Cadeddu, R. D. Demaree, H. A. Basile, R. H. Taylor, L. L. Whitcomb, W. N. Sharpe, L. R. Kavoussi, “An Efficient Needle Injection Technique and Radiological Guidance Method for Percutaneous Procedures”, *Lecture Notes in Computer Science*, CVRMed-MRCAS, Springer-Verlag, vol. 1205, pp. 295-298, 1997.
12. D. Stoianovici, L. L. Whitcomb, J. H. Anderson, R. H. Taylor, and L. R. Kavoussi, “A Modular Surgical Robotic System for Image-Guided Percutaneous Procedures”, Int. Conf. *Medical Image Computing and Computer-Assisted Intervention* (MICCAI), Springer-Verlag, vol. 1496, pp. 404-410, 1998.
13. R. H. Taylor, P. Jensen, L. Whitcomb, A. Barnes, R. Kumar, D. Stoianovici, P. Gupta, Z. Wang, E. deJuan, and L. Kavoussi, “A Steady-Hand Robotic System for Microsurgical Augmentation”, International Journal of Robotics Research, **18**(12), pp. 1201-1210, Dec. 1999.
14. J. Yanof, J. Haaga, P. Klahr, C. Bauer, D. Nakamoto, A. Chaturvedi, and R. Bruce, “CT-integrated robot for interventional procedures: Preliminary experiment and computer-human interfaces”, Computer Aided Surgery, vol. **6**, pp. 352-359, 2001.
15. K, Masamune, G. Fichtinger, A. Patriciu, R. C. Susil, R. H. Taylor, L. R. Kavoussi, J. H. Anderson, I. Sakuma, T. Dohi, and D. Stoianovici, “System for robotically assisted percutaneous procedures with computed tomography guidance”, Computer Aided Surgery, **6**(6), pp. 370-383, 2001.
16. R. C. Susil, J. H. Anderson, R. H. Taylor, “A Single Image Registration Method for CT-Guided Interventions”, *Lecture Notes in Computer Science*, MICCAI’99, Springer-Verlag, vol. 1679, pp. 798-808, 1999.
17. G. Fichtinger, T. L. DeWeese, A. Patriciu, A. Tanacs, D. Mazilu, J. H. Anderson, K. Masamune, R. H. Taylor, and D. Stoianovici, “System for robotically assisted prostate biopsy and therapy with intraoperative CT guidance”, Acad. Radiol., **9**(1), pp. 60-74, Jan. 2002.
18. D. Stoianovici, K. Cleary, D. Mazilu, A. Patriciu, A. Stanimir, N. Craciunoiu, V. Watson and L. Kavoussi, “AcuBot: A Robotic System for Radiological Interventions”, IEEE Trans. on Robotics and Automation, **19**(5), pp. 926-930, 2003.
19. L. P. Nolte, M. A. Slomczykowski, U. Berlemann, M. J. Strauss, R. Hofstetter, D. Schlenzka, T. Laine, and T. Lund, “A new approach to computer-aided spine surgery: fluoroscopy-based surgical navigation”, Eur Spine J., **9**(7)**,** Suppl 1:S78-88, Feb. 2000.
20. S. Lavallee, P. Sautot, J. Troccaz, P. Cinquin and P. Merloz, “Computer-assisted spine surgery: a technique for accurate transpedicular screw fixation using CT data and a 3-D optical localizer”, J Image Guid Surg., **1**(1), pp. 65-73, 1995.
21. D. T. Gering, A. Nabavi, R. Kikinis, N. Hata, L. J. O'Donnell, W. E. Grimson, F. A. Jolesz, P. M. Black, and W. M. Wells, “An integrated visualization system for surgical planning and guidance using image fusion and an open MR”, Journal of Magnetic Resonance Imaging, **13**(6), pp. 967-975, 2001.
22. K. S. Arun, T. S. Huang, and S. D. Blostein. “Least-square fitting of two 3d point sets”, IEEE Trans. Pattern Anal. Machine Intell., **9**(5), pp. 698-700, 1987.
23. M.W. Spong and M. Vidyasagar, *Robot Dynamics and Control*, Hardcover, John Wiley & Sons, pp. 43, 1989.
24. J. M. Fitzpatrick, J.B. West and C. R. Jr. Maurer, “Predicting error in rigid-body point-based registration”, IEEE Trans. Medical Imaging, **17**(5), pp. 694-702, 1998.